

RADIATION-INDUCED ACOUSTIC LOSS IN
QUARTZ CRYSTALS

BY

GARY EDWARD AARON BERMAN

Bachelor of Arts

Trenton State College

Trenton, New Jersey

1973

Submitted to the Faculty of the Graduate College
of the Oklahoma State University
in partial fulfillment of the requirements
for the Degree of
MASTER OF SCIENCE
May, 1984

Thesis
1984
B516r
cop. 2



RADIATION-INDUCED ACOUSTIC LOSS IN
QUARTZ CRYSTALS

Thesis Approved:

Joel G. Martin

Thesis Adviser

Larry E. Halliburton

E. K. Rumba

Norman N. Durban

Dean of the Graduate College

ACKNOWLEDGMENTS

This is, to me, one of the most important sections and potentially the longest portion of this thesis. Many people have contributed both directly and indirectly, but time and length dictate limits, so I want to explicitly mention the following people.

First and foremost I want to thank Dr. J. J. Martin without whose constant help, support, advice, and unselfish contribution of time this would still be a dream. I am very proud to have learned from him and I owe him a great deal.

To Dr. L. E. Halliburton and Dr. E. E. Kohnke--I want to thank them both for agreeing to be on my Thesis Committee and for their friendship during my time at OSU. In addition, I would like to express my gratitude to Ms. Janet Sallee for the typing of this thesis.

Finally, I must deeply thank God, my Mother and Father, Sister and Family, Ione Gallup, Karen and Mark and various friends I have made at Oklahoma State University. It was through their constant love, support, and encouragement the dream was kept alive. I truly wish my Father was alive to see this day, but I know he is smiling in the other world.

Financial support for this work was provided by the U.S. Air Force under Contract Number F19628-83-K-0007 as monitored by A. F. Armington.

TABLE OF CONTENTS

Chapter	Page
I. INTRODUCTION.	1
Point Defects in Quartz.	2
Radiation Effects.	3
Purpose of Investigation	6
II. SAMPLE PREPARATION.	7
Series Resistance Method	14
Acoustic Loss Measuring System	20
III. RESULTS AND DISCUSSIONS	27
IV. CONCLUSIONS	43
REFERENCES	44

LIST OF FIGURES

Figure	Page
1. Schematic Diagram of the Crystal Mounting Apparatus Attached to the Cold Finger of the Cryostat.	10
2. Schematic Diagram of the Variable Temperature Cryostat Sharing All External Connections.	12
3. The Analog Equivalent Electrical Circuit of a Crystal	16
4. Block Diagram of the Series Resistance Measuring System Showing Impedance Measuring Circuit	18
5. Block Diagram of the Log-Decrement Measuring System	24
6. The Acoustic Loss, Q^{-1} , (Left Ordinate) and Resistance, Ω , (Right Ordinate) on a Log Scale Versus Temperature. The Curves Show the Results of First Annealing the Natural Quartz Crystal, #474 Then Irradiating at OSU. For the Natural Quartz Crystal #266 it Was Irradiated and Annealed at the Sandia Laboratories.	29
7. The Change in Acoustic Loss, ΔQ^{-1} , Versus Anneal Temperature on a Linear Plot for the Natural Quartz Crystal, #479. It Demonstrates the Defect is Eliminated in the 275C - 350C Range	31
8. The Production and Eventual Saturation of the Defect Responsible for the 249K Loss Peak for the Natural Quartz Crystal #266. The Linear Plot Shows the Change in Acoustic Loss, ΔQ^{-1} , Versus Radiation Exposure Time. Saturation Occurs at the 72 Second Exposure Time	34
9. The Change in Resistance, $\Delta \Omega$, on a Log Scale Versus Temperature for the Natural Quartz Crystal, #474. The Solid Curve Results From the Experimental Data (O) and Shows the Agreement Between the Experimental and Calculated (X) Data	36
10. The Resistance, Ω , of the Synthetic Quartz Crystal, 5S39, on a Log Scale Versus Temperature. The Crystal Was Initially Annealed Then Irradiated and the Result Suggests a Loss Peak Which Reaches Maximum Resistance Near 341K. This Agrees With the 340K Peak Found by Koehler and Martin	39

11. The Production and Eventual Saturation of the Defect Responsible for the 341K Loss Peak for the Synthetic Quartz Crystal, 5S39. The Linear Plot Shows the Change in Acoustic Loss, ΔQ^{-1} , Versus Radiation Exposure Time. Saturation Occurs at the 50 Second Exposure Time. 41

CHAPTER I

INTRODUCTION

Quartz, SiO_2 , crystallizes in the trigonal trapezohedral class. The z or optic axis is an axis of threefold symmetry-properties will be repeated at angles of $\pm 120^\circ$ rotation about the z-axis. It, together with crystals such as rochelle salt and tourmaline are piezoelectric. Piezoelectric or pressure electricity appears only in insulating solids. In the most basic sense, a plate cut from a piezoelectric crystal with electrodes attached serves not only as a capacitor for storing electric energy but also as a motor for turning electrical into mechanical energy and as a generator for turning mechanical energy into electrical energy. All of the applications of the piezoelectric effect depend on this motor-generator action of the crystal. In the crystal resonator, the action drives the crystal itself in mechanical vibration and the vibrating resonator loses energy by internal friction. The electrical signal is amplified and a small portion is fed back to sustain the oscillation. As an electromechanical transducer the mechanical stress set up by the piezoelectric effect drives not only the mechanical elements of the crystal but also any other mechanical elements attached to the crystal surface. For driving frequencies above about 10 kilocycles, piezoelectric crystals form the best means of transferring electrical into mechanical energy (1).

The melting point of quartz is 1750°C , its density is 2.65 g/cm^3 , and the hardness is 7 on the Mohs' scale. At atmospheric pressure, σ

(trigonal holoaxial) quartz is transformed into β (hexagonal)-high temperature-quartz at 573°C . α quartz is insoluble in ordinary acids, slightly soluble in water under high temperatures and pressures and is completely soluble in either hydrofluoric acid or hot alkaline solutions.

Quartz is mined primarily in Brazil in several different types of deposits (2). However, for most applications hydrothermally grown synthetic quartz is becoming the first choice. This is primarily due to the ease of manufacturing and higher purity content of the latter.

Synthetic quartz is grown using the hydrothermal process, from solutions, in which quartz nutrient is mixed with a mineralizer solution of Na_2CO_3 or NaOH in water (3). To improve the crystal's homogeneity a small amount of LiOH is often added (4). The reaction autoclave, is held under 2000 atm of pressure and brought slowly to $340\text{-}370^{\circ}\text{C}$. Those impurities introduced in synthetic quartz came from the starting materials, mineralizers, the lithium salt or the autoclave walls. However, the overall impurity concentration introduced in this synthetic quartz is at least an order of magnitude lower than for its natural counterpart (5).

Point Defects in Quartz

This study is primarily concerned with point defects. The principle active impurity in high quality synthetic quartz is an Aluminum 3^{+} in substituting for a silicon 4^{+} ion in the lattice. To preserve charge neutrality this substitution is charge-compensated by interstitials such as hydrogen (H^{+}) ions, by alkali-metal (M^{+}) ions such as lithium (Li^{+}) and sodium (Na^{+}) or by radiation-induced holes trapped at adjacent oxygen ions (6). Because of the strong coulombic attraction force of the interstitial ions and the holes with the aluminum, and because of the

high mobility of both the interstitial ions and the holes, these charge compensators are usually located adjacent to the substitutional aluminum ions and this gives rise to either Al-OH^- , Al-Li^+ , Al-Na^+ , or $[\text{Al}_{e^+}]^{\circ}$ centers (7).

Other defects are associated with an oxygen vacancy and having $S = \frac{1}{2}$ which are denoted as E' centers. The centers E'_1 , E'_2 , and E'_4 have been observed in quartz (8) and are generally an order of magnitude lower than those already mentioned. Another defect is an interstitial hydrogen atom, H° , which is stable to about 125°K (9).

Radiation Effects

All irradiations were made with a Van de Graaff accelerator. The irradiations were done with 1.75 - 2 MeV electrons which struck the target (resonator) directly, held by the cold finger of a cryostat, after passing through an Al foil window on the Removable Tail Assembly.

As the electron passes through the crystal it loses energy by primarily one of two ways. Either there is bremsstrahlung or excitation and ionization of bound electrons. At any energy these two processes are mutually competitive, but over particular energy intervals just one is the dominant effect. At the energies used, excitation and ionization are the primary effects (10). It should also be realized electrons are of little importance from the point of view of knock-on damage production. However, elastic collisions with nuclei in which no displacements are produced is important for electron energies <10 MeV (11). Since the electron is of such small relative mass its trajectory at the energies used is much larger than that of a heavy particle of the same energy. This results in an electron participating in many more elastic scattering

events of significantly larger angular deflection, than would a heavy particle under identical conditions. This serves to make the path followed by an electron as it traverses a crystal extremely indirect and corresponding increases the energy lost to bound electrons. The experimental observations made at OSU show that 1.75 MeV electrons penetrate to a depth of 3 mm in quartz.

Another effect occurring is the production of X-rays as the electrons travel through the Al foil. This is the Bremsstrahlung radiation and comes about whenever a charged particle moves in the field of the nucleus and is accelerated radiating electromagnetic waves. From classical theory the rate at which an accelerated charged particle radiates electromagnetic energy is given by (12)

$$\frac{\partial E}{\partial t} = \frac{2}{3} \frac{e^2 a^2}{c^3} .$$

where e is the electron charge, " a " the acceleration and " c " the speed of light. Since the acceleration,

$$a = \frac{F}{m}$$

the energy radiated is inversely proportional to the square of the mass. Consequently, I must consider the case of fast-moving electrons as compared to much more massive charged particles such as protons or alpha's, for example. Because

$$F \propto Ze$$

where Ze is the total charge of the nucleus, it can be said the rate of energy loss by radiation is proportional to Z^2 , where Z is the atomic

number of the absorbing material; i.e., Al foil. Al has a low Z value ($Z = 13$) which implies a small radiative loss and, more exactly, the ratio of the radiative energy loss to the ionization energy loss is given by (13)

$$\frac{(dE/dx)_{\text{rad}}}{(dE/dx)_{\text{coll}}} \approx \frac{EZ}{1600 mc^2}$$

where $mc^2 = .5/\text{MeV}$. Using $E = 1.75 \text{ MeV}$ and 2 MeV the ratio of losses for the two processes becomes:

$$\frac{(dE/dx)_{\text{rad}}}{(dE/dx)_{\text{coll}}} \approx \begin{cases} 2.79 \times 10^{-2}; & 1.75 \text{ MeV} \\ 3.19 \times 10^{-2}; & 2 \text{ MeV} \end{cases}$$

Consequently, x-ray production is extremely small. Due to the much greater penetration ability of x-rays, defects in the crystal are produced at greater depths. For quantum energies $> .1 \text{ MeV}$ the atomic electrons may be considered "free" and unbound (14). The striking photon makes an elastic collision with an atomic electron and is scattered through an angle θ . The energy lost by the photon appears as kinetic energy of the electron and momentum is conserved in the collision. This is Compton Scattering and for the Z value of the crystal and energy of the photons is dominant process (15). This is now equivalent to the previous process except now energetic electrons are liberated much more deeply in the crystal.

By either process the ionization process is very important. The energy given up goes to electrons and holes in the conduction band and valence band which moves through the sample and interacts with impurities and defects such as Al-Na^+ . Many, though, of these pairs just recombine.

However, it is this change of the local crystalline field, in the exchange, which changes the crystal's mechanical properties (i.e., resonant frequency, internal friction, etc.). For example, the Al-Na⁺ center is responsible for the large acoustic loss peak near 54K (16).

D. R. Koehler and J. J. Martin (17) measured the transient acoustic loss (Q^{-1}) in both synthetic and natural quartz over the temperature range 110K to 390K. They used Toyo Supreme Q quartz blanks both in the unswept and Na and Li swept versions together with natural, unswept quartz. Using, 70 ns wide x-ray pulses at 6000 Rad/pulse produced an immediate, transient acoustic loss peak centered at 360 K in the Na swept synthetic sample. At 380K the unswept and Li swept synthetic samples produced a transient loss peak on top of the broad background. There was also a rapidly increasing transient loss observed above 350K for the natural quartz sample. This suggested a peak somewhere above the 400K maximum temperature. At the completion of their irradiation series, steady state loss peaks at 305K in the Na swept synthetic sample and at 340K in the unswept and Li swept synthetic samples were observed.

Purpose of Investigation

The purpose of this investigation was firstly to confirm the production of the 304K and 340K acoustic loss peaks in synthetic quartz reported by Koehler and Martin (FCS-83). The isothermal annealing characteristics of these peaks was also investigated. A similar peak at 255K was found in natural quartz. The behavior of this peak during isothermal anneal was investigated. Lastly, this activation energy and relaxation time for the 255K peak in natural quartz are to be determined by comparing the anelastic relaxation mode with the measured curve.

CHAPTER II

SAMPLE PREPARATION

A set of 3, 5 MHz 3rd overtone plano-convex blanks were fabricated by Frequency Electronics Inc. from Toyo Supreme Q synthetic quartz. This is the Oklahoma State University Bar SQ-B. One blank was left unswept, one was Na swept and the third was Li swept. However, the blanks were inadvertently mixed at the General Electric Nuclear Division while being mounted in ceramic flat pack holders. Upon reviewing the acoustic loss versus temperature curves the synthetic quartz samples were designated 5537, Li swept; 5539, Na swept; and 5540, unswept. Due to eventual problems with electrode contacts on the ceramic flat packs the blanks were removed for final measurements.

In addition to the above samples, two Brazilian natural Quartz resonators were also available for testing using the Δ resistance and log-decrement methods. They were designated number 474 and number 266. Both are 5 MHz, 5th overtone plano-convex AT cuts mounted in "TO" type cans. They were fabricated by Western Electric and kindly loaned to us by D. R. Koehler of the Sandia National Labs.

Before using the removed blanks in the log-decrement method each resonator was thoroughly cleaned. This involved securing the blank in a custom built holder then submerging it into the well of an ultrasonic cleaner using diluted Buehler Ultramet Sonic cleaning solution for approximately two minutes. A hot water rinse follows then another rinse

in distilled water with a final mild sponging of the crystal/holder assembly before being placed into the dryer oven. The oven temperature was between 120-140°C. The holder/crystal assembly was left for 15-30 minutes before final, visual examination. If there were water spots or evidence of unremoved surface dirt the above process was repeated. If not, the crystal was mounted in preparation for acoustic loss measurements.

As mentioned earlier the flat packs were eventually disassembled and the blanks removed; then remounted. This new mounting involved placing a crystal blank in a gap holder using a parallel plate type arrangement between the PC board and base. As shown in Figure 1.

This proved a versatile arrangement since measurements could be performed with both the log-decrement and series resistance techniques. The latter only required a change in the external electric circuit.

The stainless steel variable temperature cryostat consisted of an inner variable heat leak chamber system, vacuum insulated from the surroundings. The heat leak chamber could be filled with a low molecular weight gas such as helium to facilitate rapid heat transfer while the larger, inner dewar could hold ice or liquid nitrogen. This dewar is shown in Figure 2.

The Removable Tail Assembly consisted of four windows directly in line with the crystal resonator. One window is aluminum foil while the other three are planar, Ca F_2 crystals. The latter was not used in this experiment but is for optical work.

The only disadvantage of this assembly was the mounting system for the crystal. Since the resonator blank is secured by gravity in its assembly it could be easily knocked from alignment. Consequently,

Figure 1. Schematic Diagram of the Crystal Mounting Apparatus Attached to the Cold Finger of the Cryostat

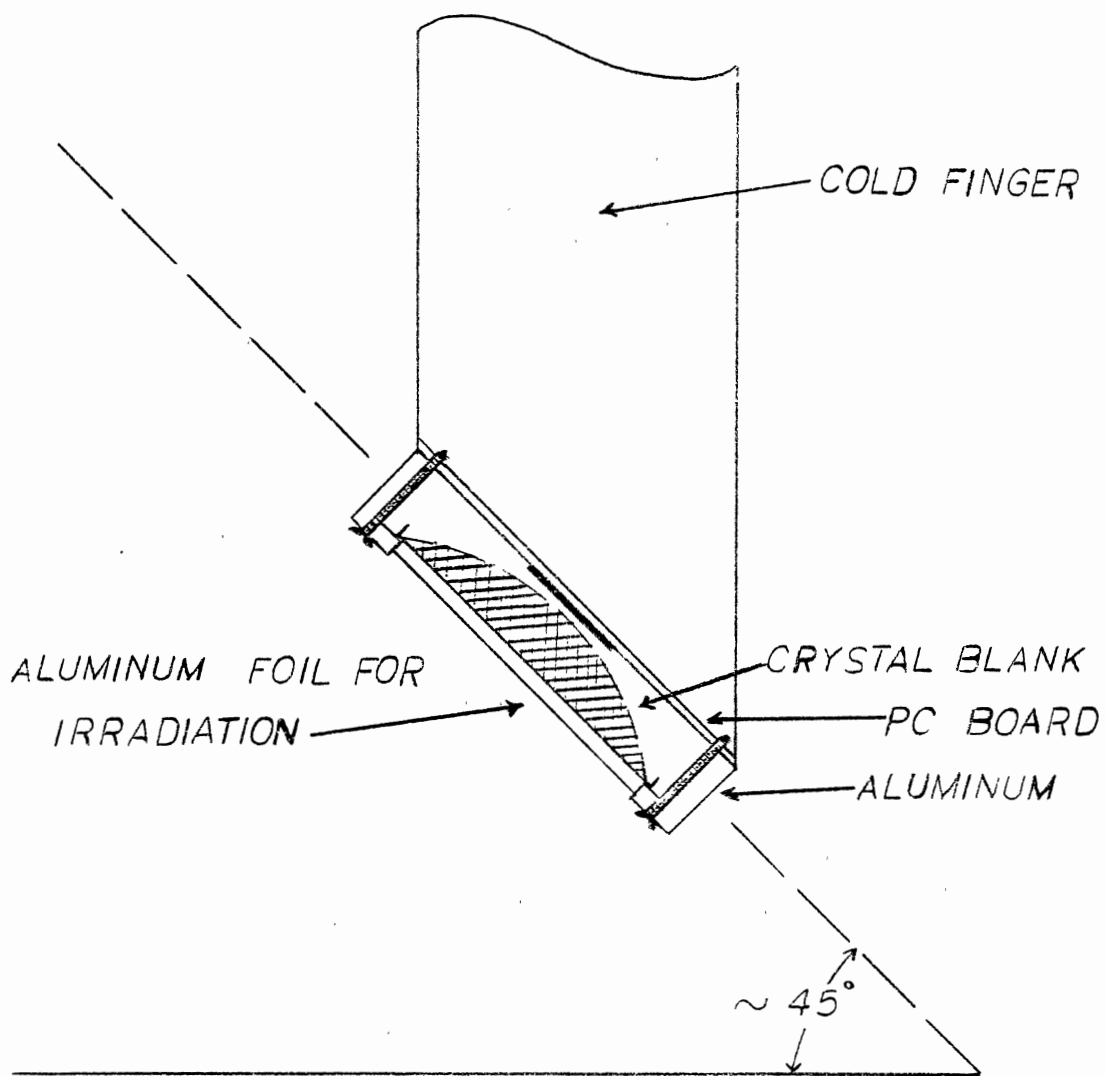
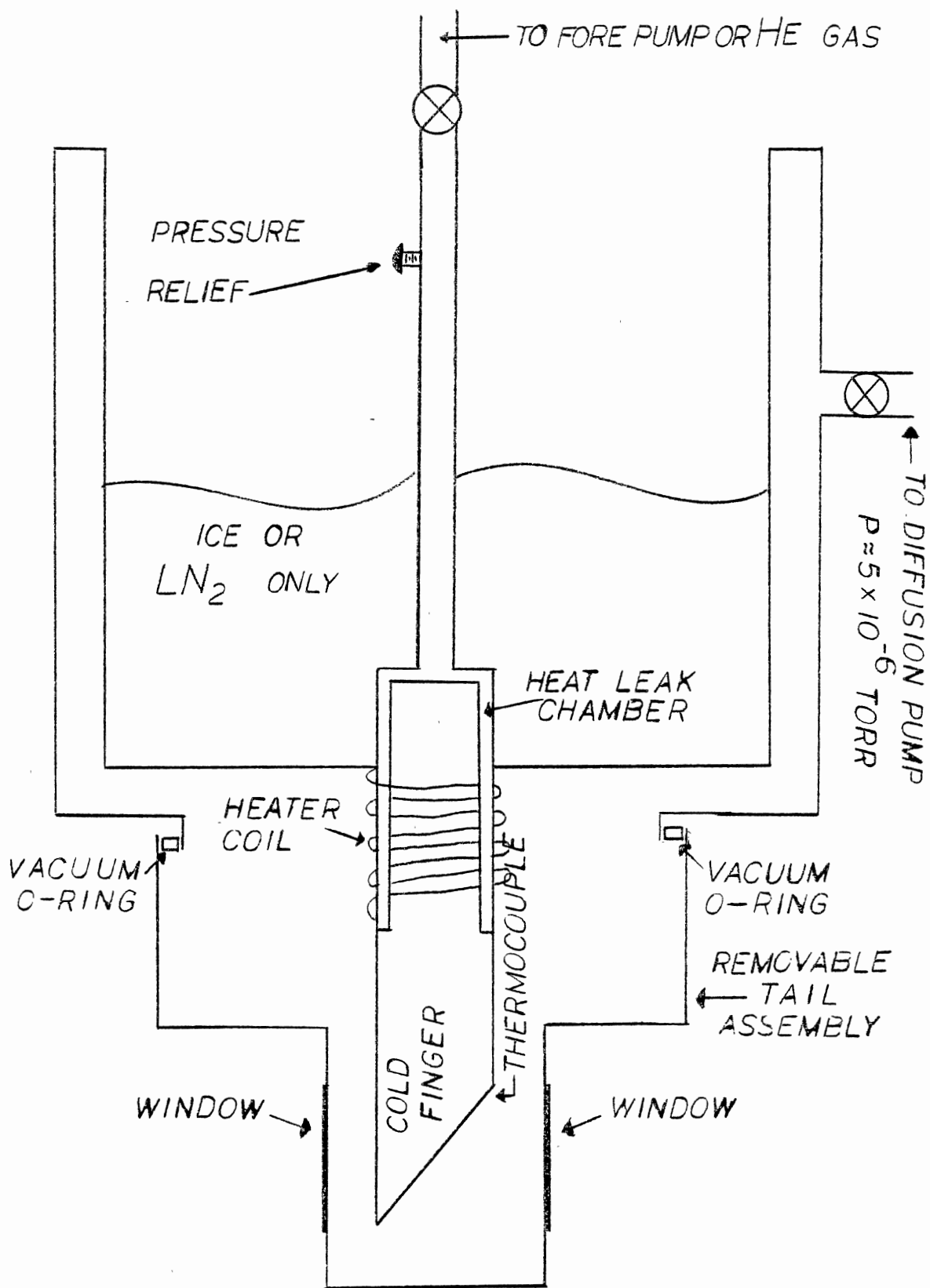


Figure 2. Schematic Diagram of the Variable Temperature Cryostat Sharing all External Connections



moving such a mounted crystal required the cryostat to be held vertically or, if tilted, tilted towards the Al foil base. Care in transport was exercised at all times.

The temperature control system consisted of an HP 6289A, DC Power Supply in line with a 30Ω constantan heater wrapped around the cold finger of the cryostat. A Digitec 268 DC Multivoltmeter measured the emf of an ice-referenced chromel-alumel thermocouple. When it was necessary to determine Q^{-1} as a function of varying temperature the power supply was adjusted in small increments of approximately .1A after setting to a starting point of, say, .5A. This allows a slow, uniform heating and though crude, worked well.

Proper procedure for cooling a crystal blank and its housing from room to liquid nitrogen temperature (77°K), for example, involved pumping on the heat leak chamber with a fore pump and on the outer dewar with a diffusion pump for several hours. At which time the heat leak chamber connecting the sample assembly on the cold finger with the cryogenic fluid in the inner dewar was filled with helium gas at room temperature. Liquid nitrogen was then poured into the inner dewar causing the sample temperature to fall rapidly to 77°K . At that temperature, the heat leak chamber is pumped out, partially disconnecting the cold finger from the bath. This allows the use of lower heater powers to achieve a desired temperature and reduces the vaporization of the cryogenic fluid in the bath. Continuous pumping on the heat leak chamber into the fore pump is necessary for stable and repeatable temperature control. If the cryostat was to be transported, say for irradiation, then valves on the body of the cryostat are closed maintaining the conditions above.

Series Resistance Method

The analog equivalent electrical circuit of a crystal was first derived by K. S. Van Dyke in 1925. Figure 3 represents the equivalent circuit.

In such a circuit C_0 represents the capacitance between the electrodes of the crystal when inactive. The inductance L_1 , capacitance C_1 and resistance R represent respectively, the electrical equivalents of the effective mass, mechanical capacitance (such as the compression of a spring) and frictional loss of the crystal when in vibration. For an appropriate frequency supplied between the terminals A and B, the reactance of L_1 , C_1 , and C_0 , will form a parallel resonant circuit. Minimum total current will occur at resonance together with maximum impedance. L_1 and C_1 can also form a series resonant circuit, which is the quoted appropriate frequency of our crystals. It is also through series resonance that the main properties of the crystal are realized.

For series resonance, the impedance is a minimum and the current is maximum. Consequently, when a crystal resonator is made an element of a circuit such as in Figure 4, a vector voltmeter can easily detect a voltage and phase difference between the input and output radio-frequency signal.

The circuit consists of an EXACT, Model 801 Frequency Synthesizer in line with a signal splitter to separate part of the synthesizer's output. One-half of the signal goes to the Heath SM-118A Frequency Counter which is used to display the output frequency. The other half of the signal goes directly to the circuit. The resistors R_1 were chosen to be 40Ω each while those in the pi network, R_2 , were 10Ω each. The series combination of R_1 and R_2 approximately matches the 50 ohm transmission

Figure 3. The Analog Equivalent Electrical Circuit of a Crystal

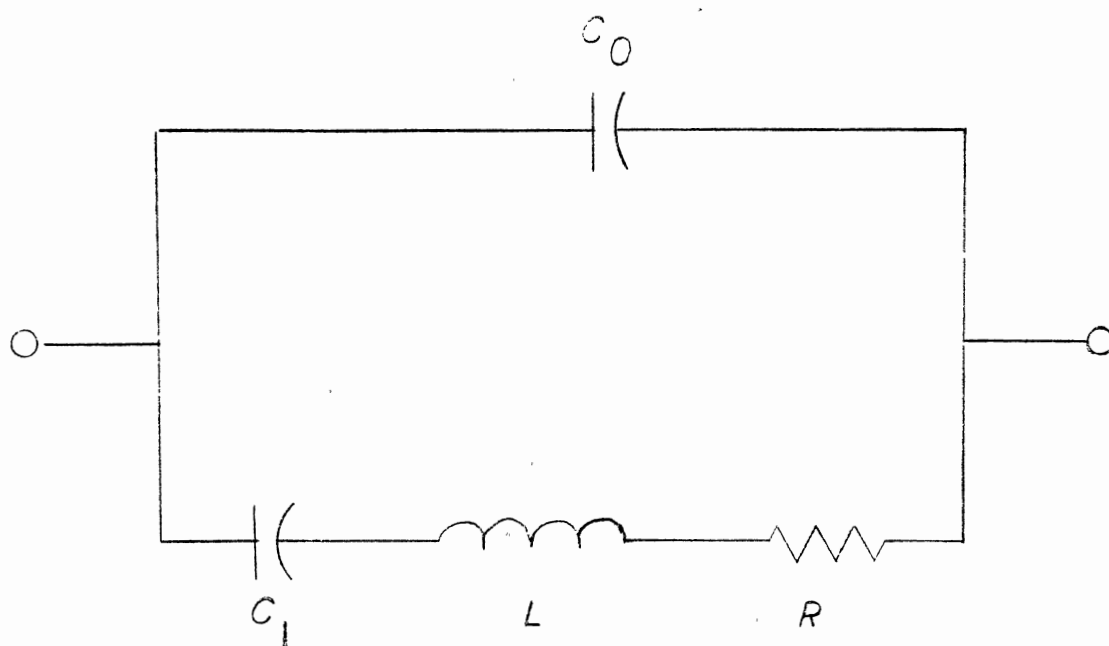
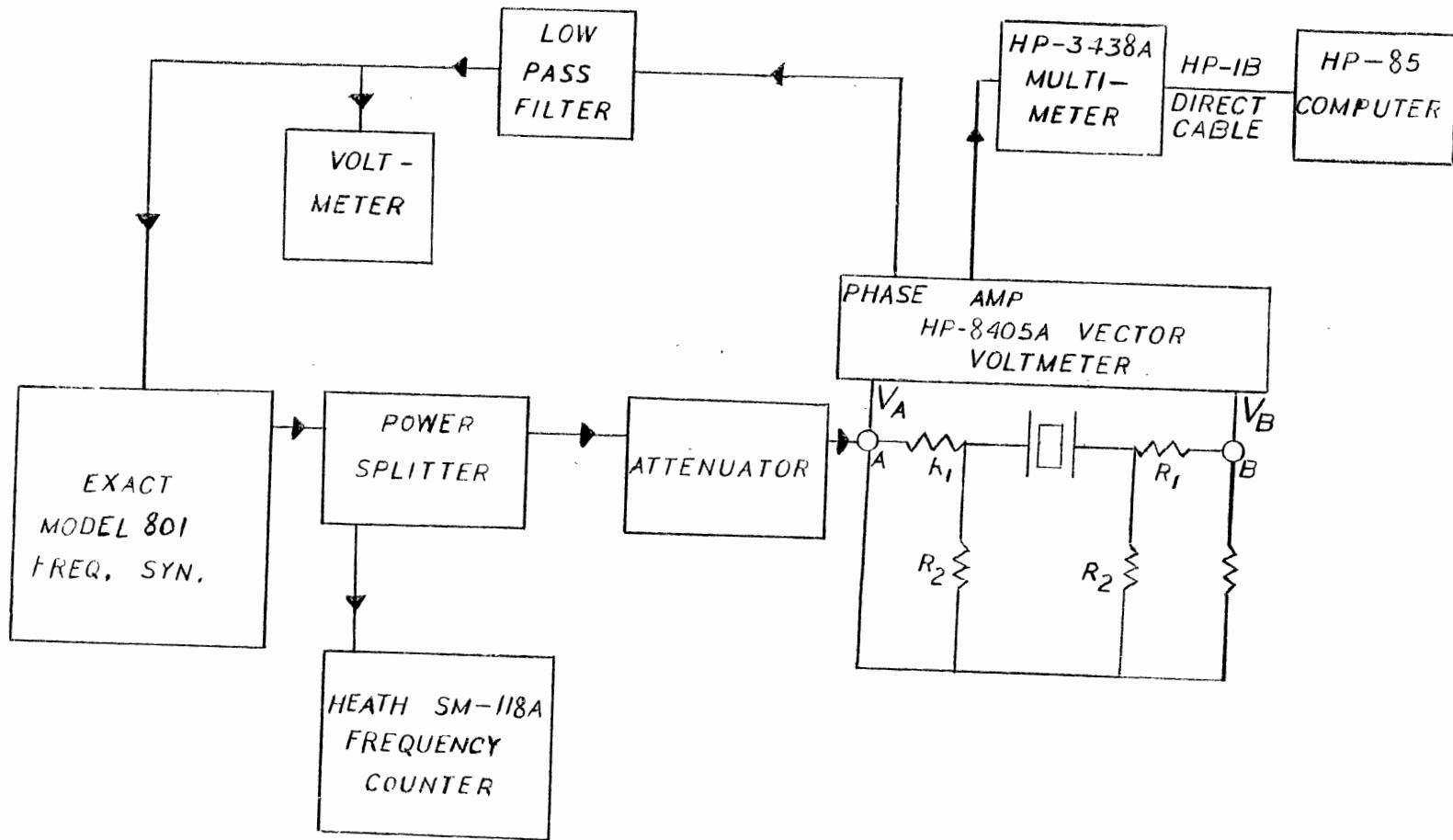


Figure 4. Block Diagram of the Series Resistance
Measuring System Showing Impedance
Measuring Circuit



lines used in this experiment. The divider network formed by R_1 and R_2 reduces the effect of crystal impedance changes on the load seen by the source. To prevent unwanted reflections a 50Ω load (resistor) was added. A Hewlett Packard, Model 8405A Vector Voltmeter (VVM) displayed the input amplitude of the applied radio frequency on channel A while channel B determined the phase difference between the two channels and the amplitude of the voltage at this point. The VVM then outputs a DC voltage proportional to the AC voltage, V_A , which is measured by the Hewlett Packard 3438A Multimeter. This information is converged to an Hewlett Packard 85 computer through the IEEE-488 (HP-IB) Interface the phase meter reading, like the amplitude reading, outputs a DC voltage proportional to the phase value. Zero volts corresponds to zero phase reading. To help stabilize the phase readings over varied temperature and transient frequency (integrator) shifts in the crystal upon irradiation a phase-locked-loop was added. A low pass filter (time constant .1 second) added to the loop circuit further enhanced the phase stability. A converted DC microampere, Simpson meter displayed the output, DC phase voltage.

The crystal resonator was originally mounted in a ceramic flatpack holder. The entire circuit was then mounted in an Al box with an Al top. A hole in the cover allowed irradiation of the resonator while protecting the rest of the circuit. However, the electrode contacts to the flat peaks failed so they were disassembled and the crystals mounted in a variable temperature crystal. Just prior to this failure, crystal 5S39 was irradiated and its series impedance measured both before, during, and after irradiation as a function of temperature. The "TO" type can, crystal 474 was also measured using this technique but was

mounted in the variable temperature cryostat.

For either crystal and mounting system, measurement of the variable series impedance was the same. Firstly, the synthesizer was adjusted to the correct series resonance frequency--which produced zero degree phase and maximum voltage on channel B of the VVM, then voltages V_A and V_B were recorded. Once V_A was set it was not touched so at each specific temperature recorded only the measurement of V_B need be reported. Such a procedure would give data to produce a graph of R versus temperature. Then the crystal was irradiated at the correct resonant frequency (which may shift somewhat due to transients), beam current, temperature, beam energy, distance, and time. Typical beam factors were $2\mu\text{A}$ current at approximately 1.85 MeV energy for 2 second pulses. When this series of experiments was completed a new spectrum of R vs temperature was run to observe an increase in the magnitude of the crystal impedance.

Circuit analysis performed on the network in series resonance (0° phase on channel B) gives the crystal impedance as,

$$Z_{\text{crystal}} = \left(1.04 \frac{V_A}{V_B}\right)\Omega - 17.52\Omega$$

for the values of R_1 , R_2 used.

Acoustic Loss Measuring System

The acoustic loss (internal friction or Q^{-1}) was measured as functions of temperatures and radiation dose for both synthetic and natural quartz samples.

The model that may be used to represent a resonant system with one degree of freedom is the mass/spring harmonic oscillator. The force,

F_s , that the mass exerts on the spring may be written as

$$F_s = kx \quad (1)$$

where k is the spring constant. However, for an anelastic specimen such as a quartz oscillator crystal damping is present. The damping or internal friction can be treated by means of a complex spring constant k^* , therefore, I can write,

$$F_s = k^*x = k_1(1 + i \tan\phi)x \quad (2)$$

where ϕ represents the angle by which the strain lags behind the stress and is known as the loss angle while k_1 is a function of frequency (18).

Now, in the absence of a forced-vibration, such as a free decay, the equation of motion of the system is

$$m\ddot{x} = -F_s = -k_1(1 + i \tan\phi)x$$

or

$$m\ddot{x} + k_1(1 + i \tan\phi)x = 0 \quad (3)$$

The solution of Equation (3) is

$$x = x_0 \exp(iw^*t); w^* = w_0(1 + i\delta/2\pi) \quad (4)$$

or

$$x = x_0 \exp(-\delta f_0 t) \exp(iw_0 t) \equiv A(t) \exp(iw_0 t) \quad (5)$$

where $f_0 = w_0/2\pi$ is the frequency, δ is a constant and $A(t) = x_0 \exp(-\delta f_0 t)$ is the decaying amplitude or envelope of the oscillation.

Thus, the problem is to measure the exponential decay reciprocal time, τ^{-1} , where $\tau^{-1} = \delta f_0$. This is done by now driving the crystal at its resonant frequency for approximately 30 - 40 ms. The drive is then turned off and the amplitude is measured during the free decay. By substituting the solution (Eqn. 4) back into the differential equation of motion it can be shown that for small angle, ϕ , that

$$\delta \approx \pi \phi . \quad (6)$$

The envelope of the freely decaying voltage is given by

$$v = v_0 \exp(-t/t_0) \quad (7)$$

where t_0 is the time constant of the decay.

Figure 5 shows the experimental set up used to drive the crystal and to measure the free decay time, t_0 . For convenience the level detectors were set to stop the timer when the signal had fallen to one-half of the start value. Thus, the timer reads $t_{1/2}$, the time for the amplitude to decrease by a factor of two. From Equation (7) this gives

$$t_0 = t_{1/2} / \ln 2 .$$

Comparing Equation (7) with Equation (5) I obtain

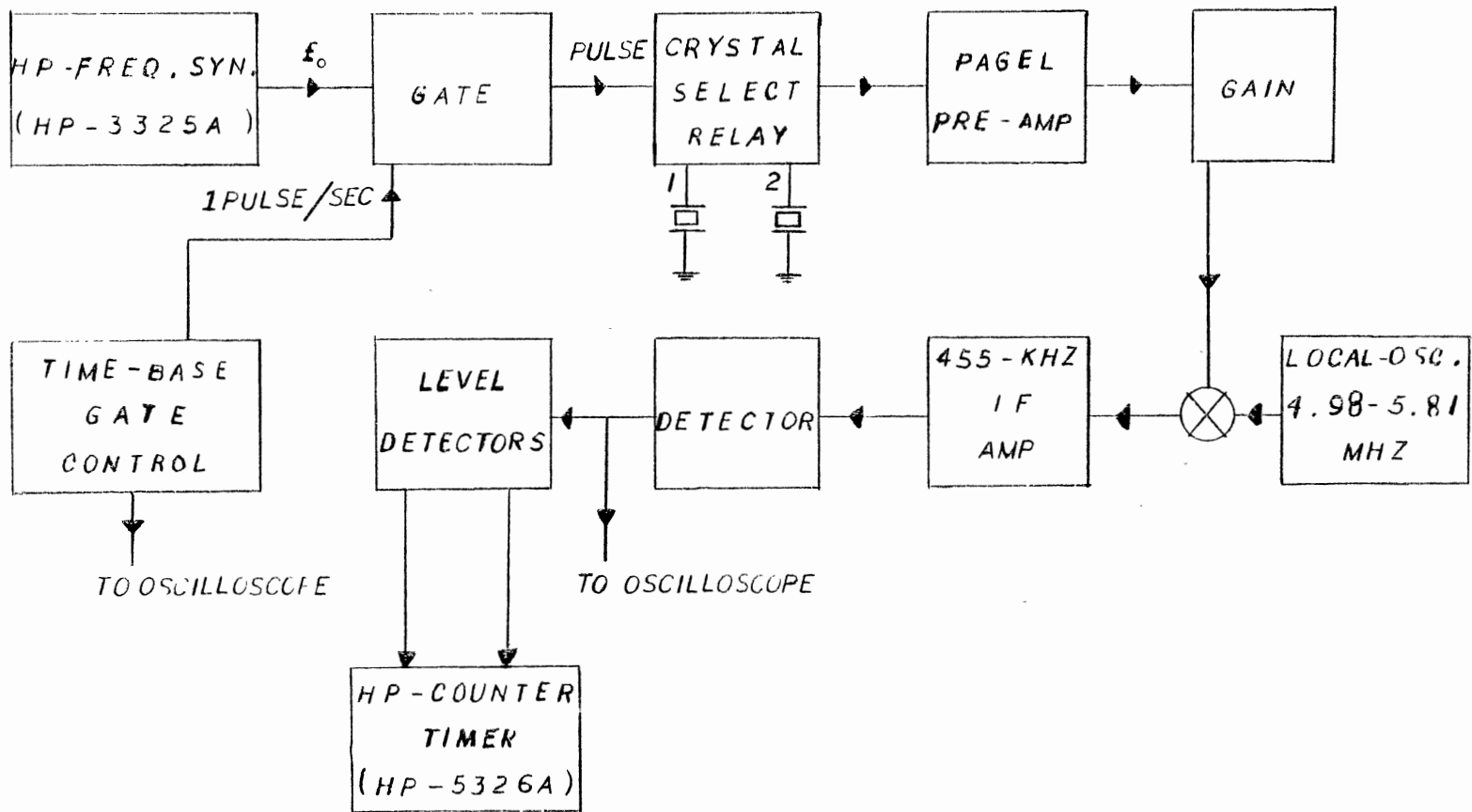
$$\delta f_0 = \frac{1}{t_0} \quad (8)$$

but

$$\delta \approx \pi \phi \approx \pi Q^{-1} \quad (\phi \text{ small}) \quad (9)$$

∴

Figure 5. Block Diagram of the Log-Decrement Measuring System



The acoustic loss, Q^{-1} , becomes

$$Q^{-1} \approx \frac{1}{\pi \delta} = \frac{1}{\pi t_o f_o} = \frac{\ln 2}{\pi f_o t_{1/2}} . \quad (10)$$

The equipment for the procedure requires the receiver, a frequency synthesizer (HP-3325A), a storage oscilloscope (Tetronix 5441), a counter/timer (HP-5326A) and the crystal resonator. The latter is excited at resonance for approximately 40 ms then freely decays at which time the timer/counter displays $t_{1/2}$.

The block diagram of the system is shown in Figure 5. The output of the synthesizer at the crystal resonant frequency, f_o , is applied to the crystal by the rf gate. For approximately 40 ms the gate is opened while the drive signal is usually repeated every second. The relay selects the desired crystal.

When the gate closes the resonator freely decays exponentially at its resonant frequency. This decaying radio frequency voltage is amplified and detected by a superheterodyne receiver with a linear AC-DC converter. The receiver uses an IF frequency of 455 kHz so the output represents the difference between the crystal and the local oscillator which gives another exponentially decaying waveform. The detector output which is the envelope of the decaying signal is fed to the storage oscilloscope and to the level detector. An oscilloscope is used for tuning the synthesizer to the resonant frequency of the crystal. It will also show the presence of coupled resonator modes.

The time, $t_{1/2}$, comes from the timer/counter. When the detector (oscilloscope) signal falls from a maximum value (15 volts, in this case) to a lower pre-set level (8 volts), it triggers the start of the timer.

As the signal further decays to 4 volts it stops the timer. The counter then displays the value, $t_{1/2}$.

The crystal resonators were mounted on the cold finger of a variable temperature stainless steel liquid nitrogen cryostat. The crystals were either attached to the finger by a gap holder or came in premounted, "TO" type cans. Surrounding the cold finger/crystal resonator section is a Removable Tail Assembly. The cryostat is described in more detail under, Sample Preparation.

The measurement procedure is as follows. At a stable temperature the tuning dial of the receiver and the synthesizer are adjusted to the crystal (resonator) frequency. Next the gain, gate and repetition rate are adjusted. This should display a decaying DC pulse which is maximized by final adjustments to the receiver and synthesizer. When done properly the screen displays a DC signal, 15 volts in height, lasting for 30 to 40 ms before decaying. Measurements are taken at time intervals dependent upon the process investigated.

CHAPTER III

RESULTS AND DISCUSSIONS

The equivalent technique of measuring the series resistance and acoustic loss were used to characterize properties of the crystal resonators. Figure 6 shows the loss peaks for the natural quartz crystals, number (#) 266 and number (#) 474, using the combination of techniques.

Figure 6 represents the acoustic loss (Q^{-1}) versus temperature for crystal #474. This crystal was first annealed at 400C for approximately ten minutes then irradiated at Oklahoma State University. However, prior to this it was irradiated at Sandia National Laboratories. The series resistance (R_s) versus temperature for crystal #266 are, respectively, for an irradiation at the Sandia National Laboratories then an anneal at 435C.

As shown by Figure 6 the radiation induced loss peaks for the two techniques give the same results. The peak occurs at 249K which is in good agreement with the 250K peak observed by Koehler and Martin (19) for the same crystal, #474.

Figure 7 is the isochronal anneal data of linear ΔQ^{-1} versus temperature for crystal #474. The change in acoustic loss represents the difference in Q^{-1} for a prior irradiation at the Sandia Laboratories and the subsequent acoustic loss at the peak temperature (249K) for a series of anneals performed at Oklahoma State University. This graph demonstrates the decay of the loss peak for the anneal temperatures 250C,

Figure 6. The Acoustic Loss, Q^{-1} , (Left Ordinate) and Resistance, Ω , (Right Ordinate) on a Log Scale Versus Temperature. The Curves Show the Results of First Annealing the Natural Quartz Crystal, #474 Then Irradiating at OSU. For the Natural Quartz Crystal #266 it Was Irradiated and Annealed at the Sandia Laboratories

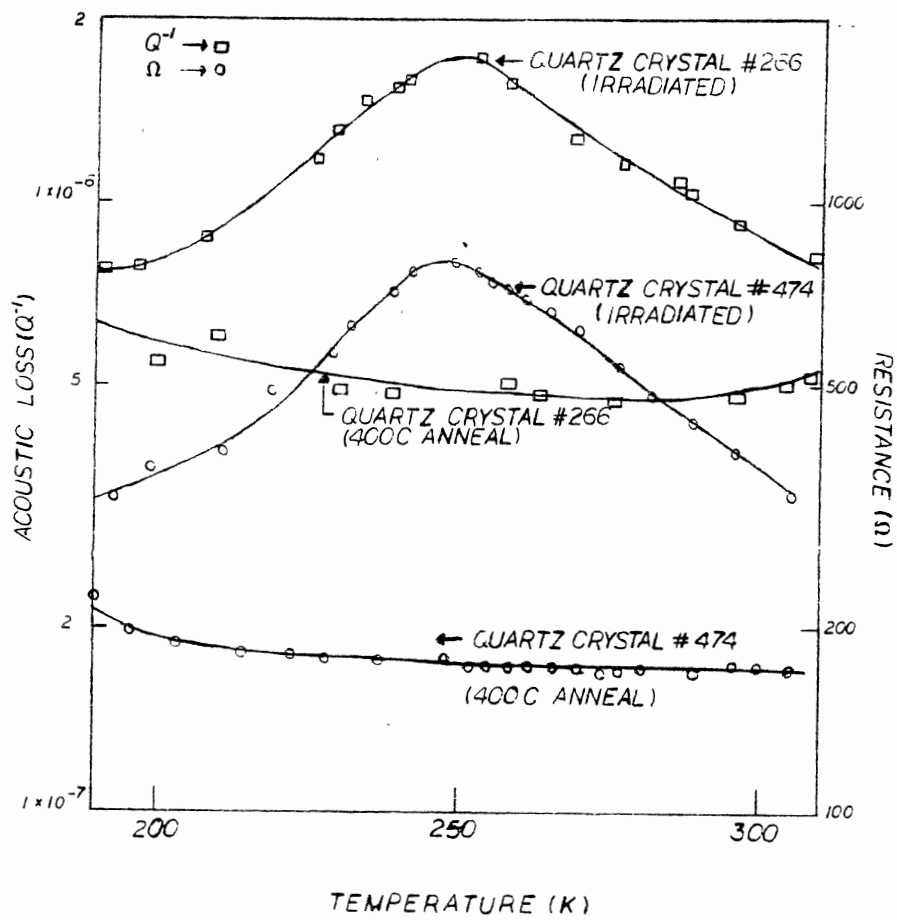
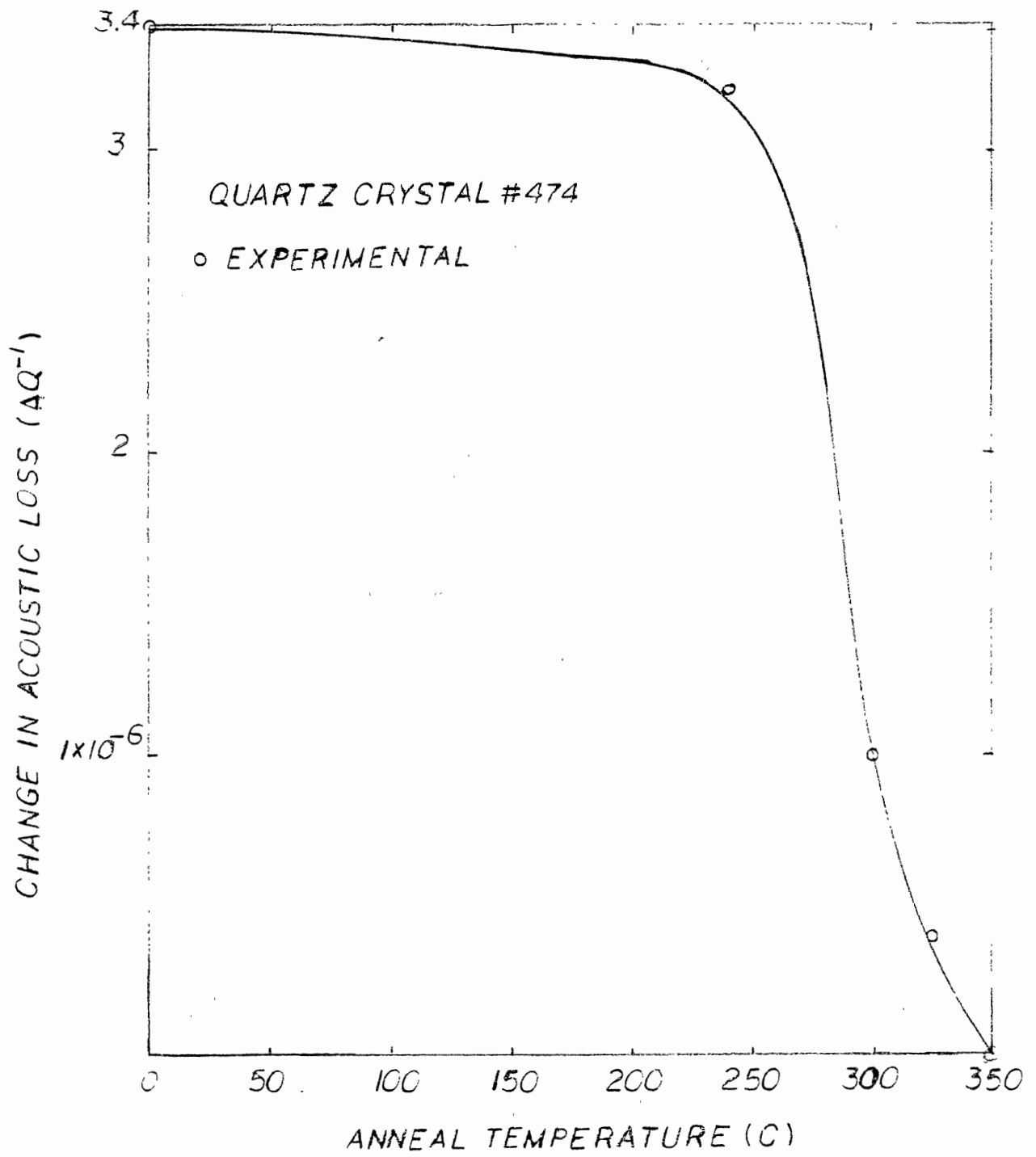


Figure 7. The Change in Acoustic Loss, ΔQ^{-i} ,
Versus Anneal Temperature on a
Linear Plot for the Natural Quartz
Crystal, #479. It Demonstrates
the Defect is Eliminated in the
275C - 350C Range



300C, 325C, 350C.

Figure 8, shows the production of the defect responsible for the 249K peak. This graph is a plot of ΔQ^{-1} versus irradiation time for the "TO" type can oscillator, #266. The crystal was mounted in the low temperature cryostat, 6 inches from the Van de Graaff window, exposed to a beam energy of 1.8 MeV and beam current of $2\mu\text{A}$. The exposure began at 10.75C and ended at 12.25C. This is not at the peak, but it is still on the loss curve and was the lowest temperature easily achievable with ice. All data was recorded approximately two minutes after each irradiation to eliminate the transient Q^{-1} effects.

The anelastic loss peaks of Figure 6 are proved at half-maximum and since the peak width varies inversely as the activation energy, ΔH , a small value of this energy is expected.

Anelastic loss peaks can often be described by Equation (1),

$$\Delta Q^{-1} = \frac{D \omega \tau}{1 + (\omega \tau)^2} \quad (1)$$

where D is the relaxation strength, τ is the relaxation time of the loss process, and $\omega = 2\pi f$; f is the applied resonant frequency. While the relaxation time, itself, is given by Equation (2),

$$\tau = \tau_0 \exp(\Delta H/kT) . \quad (2)$$

the factor τ_0 is related to some fundamental "jump time" and an entropy factor (20), ΔH is the activation energy, k is Boltzmann's constant, and T is the absolute temperature. The activation energy and τ_0 were found by fitting Equation (1) and Equation (2) to the loss peak observed in crystal #474. The solid curve of Figure 9 represents the difference

Figure 8. The Production and Eventual Saturation of the Defect Responsible for the 249K Loss Peak for the Natural Quartz Crystal #266. The Linear Plot Shows the Change in Acoustic Loss, ΔQ^{-1} , Versus Radiation Exposure Time. Saturation Occurs at the 72 Second Exposure Time

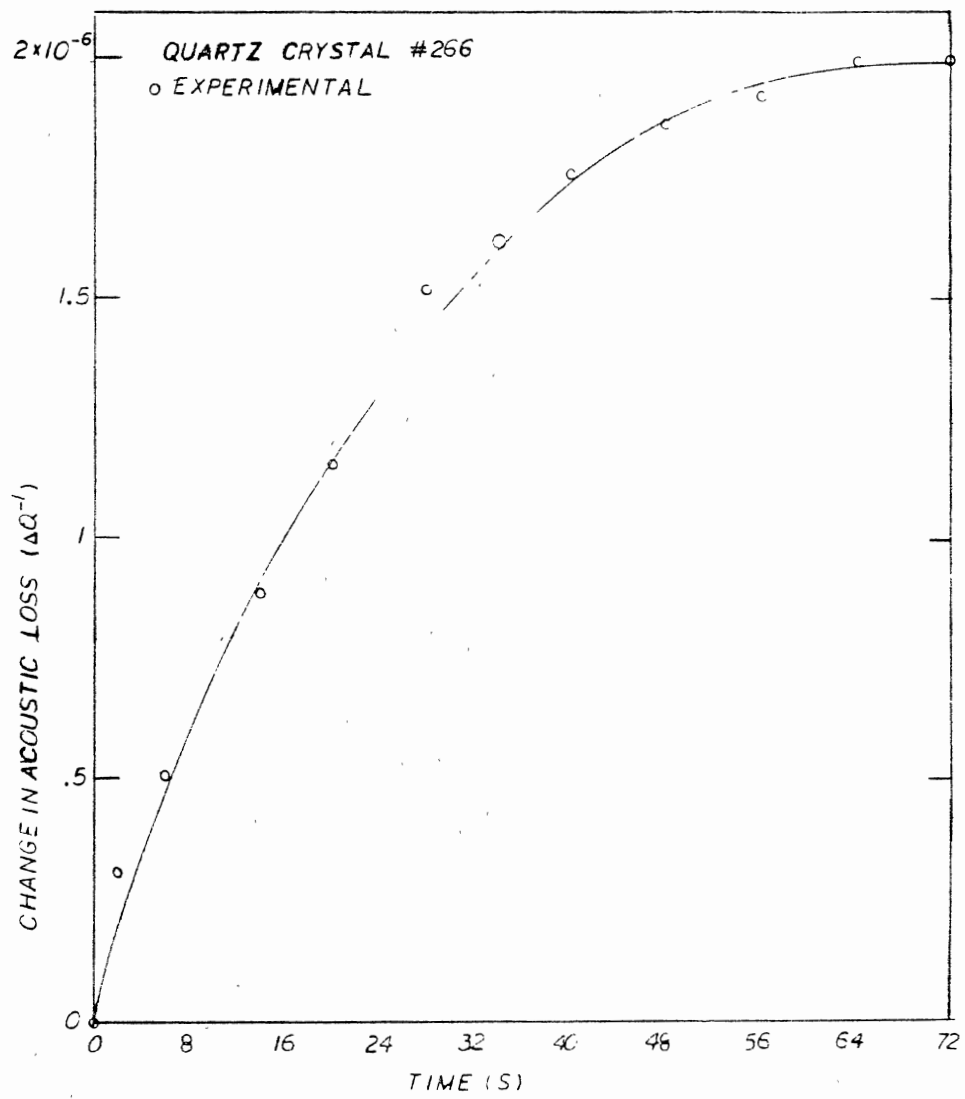
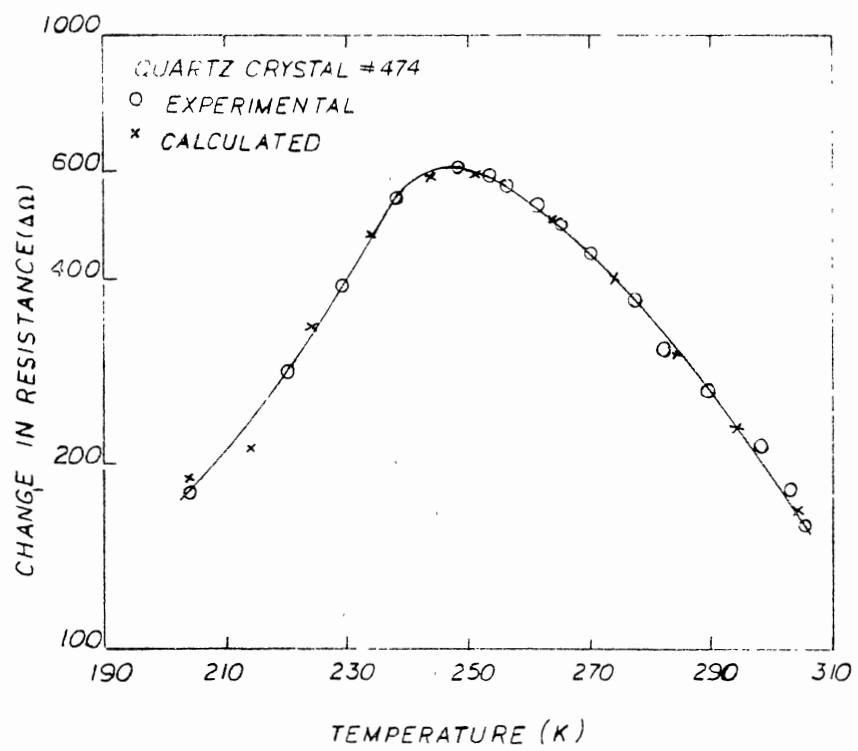


Figure 9. The Change in Resistance, $\Delta\Omega$, on a Log Scale Versus Temperature for the Natural Quartz Crystal, #474. The Solid Curve Results From the Experimental Data (O) and Shows the Agreement Between the Experimental and Calculated (X) Data



between corresponding experimental resistance values from Figure 6. It is closely approximated by $\Delta H = .224$ eV and $\tau_0 = 9.40 \times 10^{-13}$ s.

Figure 7 shows the thermal stability of the radiation-induced defects for crystal #474. Up to the 250C anneal there is very little change, but the change in acoustic loss falls rapidly to the background level for anneals in the 270C - 350C range. This is slightly above the $[Al_{e+}]^0$ center and indicates that the defect and its decay are not directly related to the Al-hole center.

The response of the crystal, #266, to irradiation shows the relatively low dose to saturate the acoustic loss. Under the prior exposure conditions, Figure 8 displays a plateau reached at approximately 56 seconds. This is greater than a four fold increase in acoustic loss over the preirradiated value.

The Toyo synthetic crystal, 5S39, was then examined under similar conditions. It was initially annealed at 450C for 10 minutes then irradiated while in the ceramic flat pack (Figure 10). The beam energy was 1.95 MeV; the pack situated 25 inches from the Van de Graaff window using a beam current of 2 μ A. Thirty-six, two second exposures were made. After this series of exposures the acoustic loss was, again, measured.

Figure 11 shows the acoustic loss of 5S39 as a function of exposure time. Originally, as received from Sandia, this crystal was mounted in a ceramic flat pack holder. However, by this time the electrodes on the peak eroded and would not allow a secure electrical contact. Consequently, the flat pack face was chemically cleaved from the main body and the crystal removed and remounted in the low temperature cryostat. This crystal/cryostat assembly was positioned six inches from the Van de

Figure 10. The Resistance, Ω , of the Synthetic Quartz Crystal, 5S39, on a Log Scale Versus Temperature. The Crystal was Initially Annealed Then Irradiated and the Result Suggests a Loss Peak Which Reaches Maximum Resistance Near 341K. This Agrees With the 340K Peak Found by Koehler and Martin

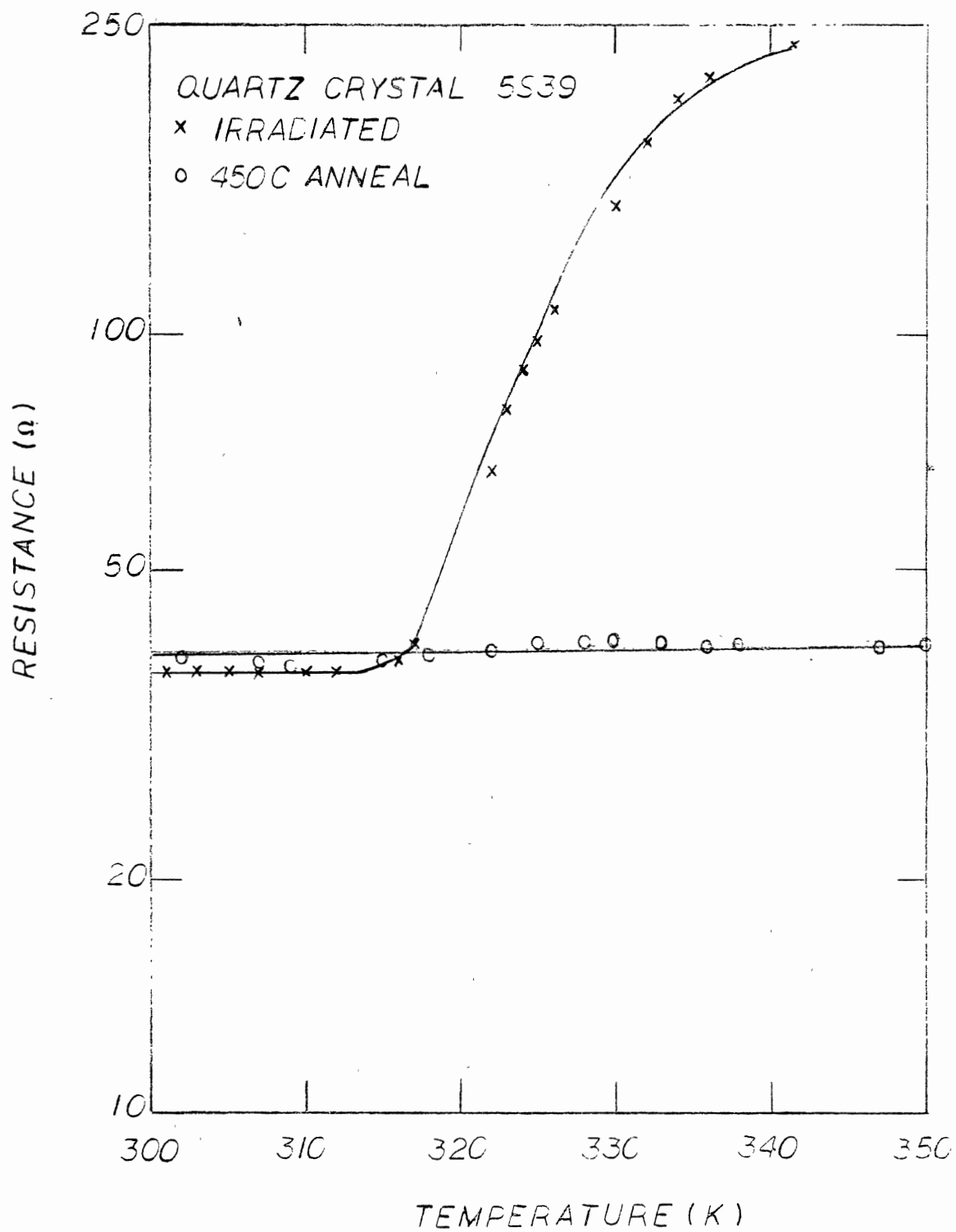
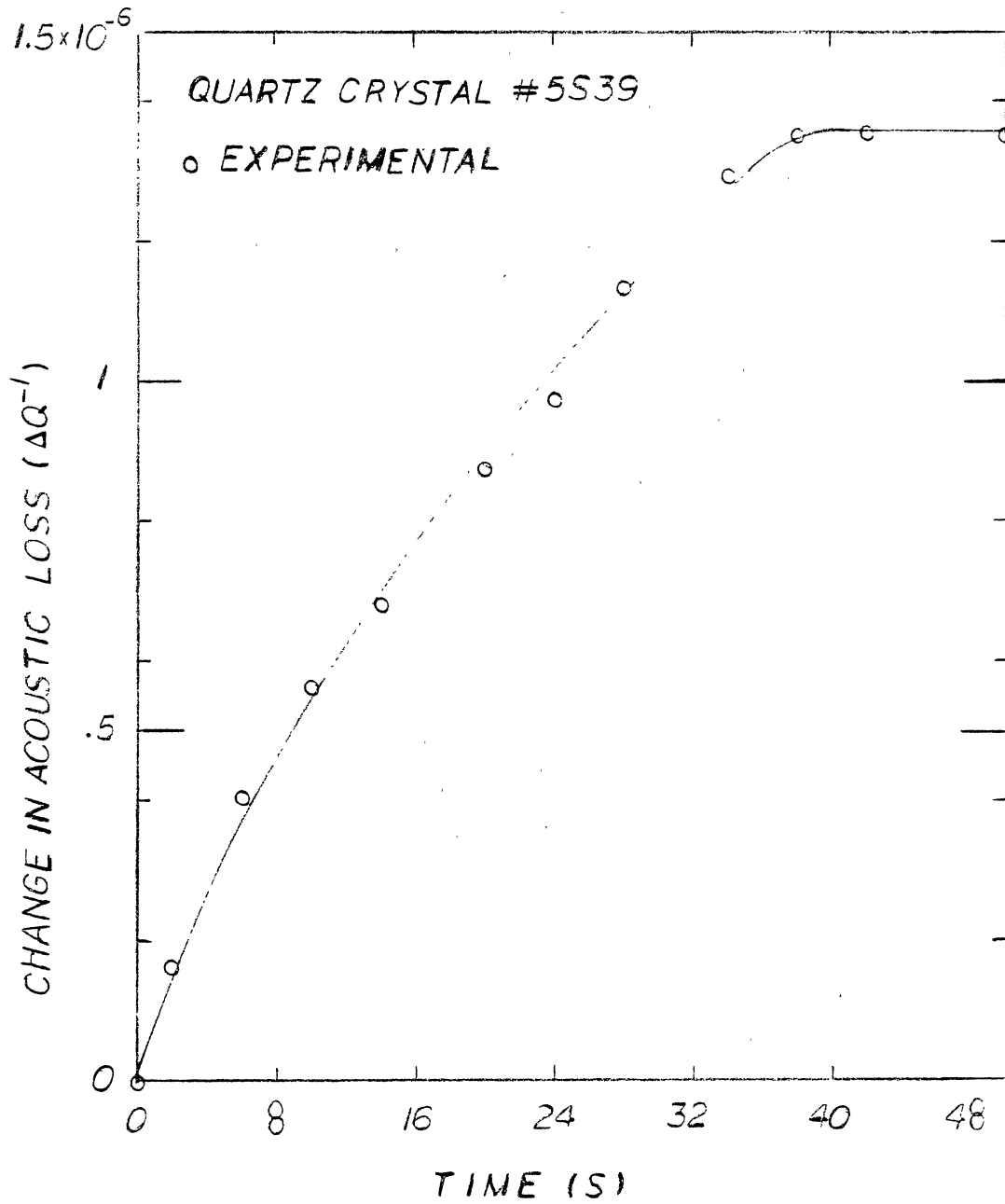


Figure 11. The Production and Eventual Saturation of the Defect Responsible for the 341K Loss Peak for the Synthetic Quartz Crystal, 5S39. The Linear Plot Shows the Change in Acoustic Loss, ΔQ^{-1} , Versus Radiation Exposure Time. Saturation Occurs at the 50 Second Exposure Time



Graaff window. The initial exposure temperature occurred at 332K at a beam energy of 1.75 MeV and current of $1\mu\text{A} - 2\mu\text{A}$. By the 50 second exposure, crystal temperature rose to 335K.

The graphs show that 5S39 behaves similarly to the natural quartz pair. Radiation exposure produces a steady state loss peak which appears to be leveling off at approximately 342K. Unfortunately, due to limitations in the heating system it was not possible to reach higher temperatures but, again, this agrees with the 340K peak found by Koehler and Martin for the same crystal. The growth of this loose peak and its production follow equal suit. Figure 11, appears to be leveling out and stabilizing at 46 seconds which is similar to crystal #266. The magnitudes of the loss for the synthetic crystal, 5S39, and the natural quartz crystal, #266, are similar for the same dose. This implies the defects for the two crystals are probably closely related but, as yet, still unknown.

CHAPTER IV

CONCLUSIONS

It was found that the temperature of the steady state radiation induced acoustic loss peak for the natural quartz samples, #266 and #474, as well as for the synthetic crystal, 5S39, agree with the respective temperatures of 250K and 340K as found by Koehler and Martin. Furthermore, the defect responsible for the 250K and 340K centered peak saturates the acoustic loss at approximately equal dose levels and exposure time for #266 and 5S39. This occurred at 56 seconds and 50 seconds, respectively. The magnitude of these losses are also similar for the two crystals so the defects are probably closely related. An activation energy of $\Delta H = .224$ eV and a "jump time" of $\tau_0 = 9.40 \times 10^{-13}$ s was calculated from the experimental data of the natural quartz crystal, #474. Koehler and Martin found that $\Delta H = .35$ eV and $\tau_0 = 2.09 \times 10^{-13}$ s fits the 340K peak of the synthetic quartz crystal, 5S39.

The results of the isochronal anneals illustrates the defect responsible for the 249K peak in the natural crystal, #474, is unstable at relatively low temperatures. It completely anneals out in the 275C - 350C range and falls off rapidly past 250C. Since the annealing temperature of this defect is slightly above that for the Al-hole center, the two defects are probably not related.

REFERENCES

1. Mason, W. P., Piezoelectric Crystals and Their Application to Ultrasonics (D. Van Nostrand, New York, 1950), p. 79.
2. King, J. C., A. A. Ballman and R. A. Landise, J. Phys. Chem. Solids, 23, 1019 (1962).
3. Armington, A. F., A. Kahan and F. K. Euler. ETS Technical Memorandum No. 3, Solid State Division, Deputy for Electronic Technology, RADC, Hanscomb AFB, Mass. 01731, September 1976.
4. Mason, W. P., Piezoelectric Crystals and Their Application to Ultrasonics (D. Van Nostrand, New York, 1950), p. 82.
5. Ibid., p. 82.
6. Jalilian-Nosraty, M., and J. J. Martin, J. Appl. Phys. 52, 785 (1981).
7. Halliburton, L. E., N. Koumvakalis, M. E. Markes and J. J. Martin, J. Appl. Phys. 52, 3565 (1981).
8. Doherty, Steven, "Radiation Effects in Quartz Resonators." (Unpub. Ph.D. Thesis, Oklahoma State University, 1980), p. 15.
9. Ibid., p. 16.
10. Chadderton, L. T., Radiation Damage in Crystals (John Wiley and Sons, Inc., New York, 1965), p. 5.
11. Ibid., p. 10.
12. Arya, A. P., Fundamentals of Nuclear Physics (Allyn and Bacon, Inc., Boston, 1970), p. 237.
13. Ibid., p. 238.
14. Chadderton, L. T., Radiation Damage in Crystals (John Wiley and Sons, Inc., New York, 1965), p. 166.
15. Ibid., p. 168.
16. Koehler, D. R. and J. J. Martin, Radiation Induced Transient Acoustic Loss in Quartz Crystals, Proc. 37th Ann. Freq. Control Symposium, USAERADCOM, Ft. Monmouth, N.J., p. 131, 1983.

17. Ibid., p. 1.
18. Nowick, A. S. and B. S. Berry, An Elastic Relaxation in Crystalline Solids (Academic Press, New York, 1972), p. 20.
19. Koehler, D. R. and J. J. Martin, Radiation Induced Transient Acoustic Loss in Quartz Crystals, Proc. 37th Ann. Freq. Control Symposium, USAERADCOM, Ft. Monmouth, N.J., p. 132, 1983.
20. Fraser, D. B., Physical Acoustics, Vol. 5, W. P. Mason, Ed. (Academic Press, New York, 1968), p. 65.

VITA 2

Gary Edward Aaron Berman

Candidate for the Degree of

Master of Science

Thesis: RADIATION INDUCED ACOUSTIC LOSS IN QUARTZ CRYSTALS

Major Field: Physics

Biographical:

Personal Data: Born in Trenton, New Jersey, June 27, 1951, the son of Aaron and Rosalie Berman.

Education: Graduated from Hamilton High (West), Trenton, New Jersey, in 1969; received the Bachelor of Arts in 1973 from Trenton State College; completed the requirements for the degree of Master of Science at Oklahoma State University, Stillwater, Oklahoma, in May, 1984.